Computational Imaging Systems for Iris Recognition

Robert Plemmons[*a], Michael Horvath[a], Emily Leonhardt[a], Paul Pauca[a], Sudhakar Prasad[b], Stephen Robinson[a], Harsha Setty[a], Todd Torgersen[a], Joeseph van der Gracht[c], Edward Dowski[d], Ramkumar Narayanswamy[d], Paulo E. X. Silveira[d]

[a]Wake Forest University; [b]University of New Mexico; [c]HoloSpex, Inc.; [d]CDM Optics, Inc.

ABSTRACT

Computational imaging systems are modern systems that consist of generalized aspheric optics and image processing capability. These systems can be optimized to greatly increase the performance above systems consisting solely of traditional optics. Computational imaging technology can be used to advantage in iris recognition applications. A major difficulty in current iris recognition systems is a very shallow depth-of-field that limits system usability and increases system complexity. We first review some current iris recognition algorithms, and then describe computational imaging approaches to iris recognition using cubic phase wavefront encoding. These new approaches can greatly increase the depth-of-field over that possible with traditional optics, while keeping sufficient recognition accuracy. In these approaches the combination of optics, detectors, and image processing all contribute to the iris recognition accuracy and efficiency. We describe different optimization methods for designing the optics and the image processing algorithms, and provide laboratory and simulation results from applying these systems and results on restoring the intermediate phase encoded images using both direct Wiener filter and iterative conjugate gradient methods.

Keywords: biometrics, iris recognition, high performance imaging, extended depth-of-field, pattern recognition, feature extraction, image restoration

1. INTRODUCTION

Reliable automatic recognition of individuals has long been an important goal, and it has taken on new importance in recent years. The use of biometric signatures, instead of tokens such as identification cards or computer passwords, continues to gain increasing attention as a means of identification and verification of individuals for controlling access to secured areas, materials, or systems. A wide variety of biometrics has been considered over the years in support of these challenges. Viable biometric signatures include those based on finger prints, facial features, hand shape, voice, automated recognition of retinal vasculature, and the iris. The iris is an overt body that is available for remote (i.e., noninvasive) assessment. The variability of features of any one iris is well enough constrained to make possible a fully automated recognition and verification system based upon machine vision, as initially described in a fundamental paper by John Daugman from Cambridge University [1]. For example, even identical twins have distinct iris features.

The iris is an annular area between the pupil and the white sclera in the eye; it has a rich texture based on interlacing features, called the texture of the iris (see Figure 1). This texture is well known to provide a signature that is unique to each subject. In fact, the operating probability of false identification by the Daugman algorithm [2] can be of the order of 1 in 10^{10}. Compared with other biometric signatures mentioned above, the iris is generally considered more stable and reliable for identification [1-3].

Iris recognition is especially attractive due to the high degree of entropy per unit area of the iris, as well as the stability of the iris texture patterns with age and health conditions. A number of groups have explored iris recognition algorithms and some systems have already been implemented and put into commercial practice by companies such as Iridian Technologies, Inc., whose system is based on the use of Daugman's algorithm.

* corresponding author: plemmons@wfu.edu; Computer Science and Mathematics, Wake Forest Univ., Winston Salem, NC 27109

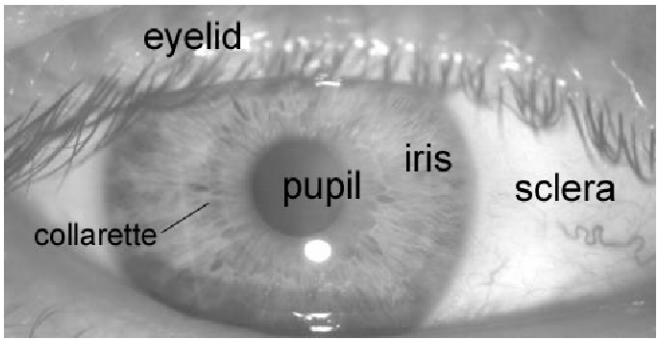

Figure 1: Anatomy of a frontal image of the eye [4].

A typical iris recognition system generally consists of the following basic modules:

I. image acquisition, iris location, and pre-processing,
II. iris texture feature extraction and signature encoding, and
III. iris signature matching for recognition or verification.

In this paper we consider the interactions and dependencies between these three modules and explore the interplay between iris sensor design, accuracy, efficiency as well as user friendliness and *acceptability of iris recognition systems*. Prior work on Module I above for iris recognition has been predicated on the assumption of traditional image gathering techniques whose aim is to produce sharply focused and visually pleasing images. Our primary goal is to modify the image acquisition to maximize the information which is directly relevant to feature extraction in Module II and the recognition task in Module III. We refer to such an enhanced system as a *computational imaging system*.

The remainder of this paper is organized as follows. In Section 2 we briefly review some of the important iris recognition systems, beginning with the seminal work of Daugman. Section 3 is concerned with the primary goal of our work, which involves increasing the imaging volume of iris recognition systems and extending the image acquisition depth-of-field. Several laboratory experiments which make use of Wiener filter restoration techniques are reported in this section, and conjugate gradient iterative methods are investigated using simulations. Here we use, in part, a basic iris recognition executable software system for the Daugman algorithm supplied to Wake Forest by Iridian Technologies under a Cooperative Research and Development Agreement (CRADA). In Section 4 we briefly discuss some of our recent work on designing new computational imaging systems for iris recognition, as well as other applications. Some conclusions and plans for future work are given in Section 5.

2. OVERVIEW OF SOME IRIS RECOGNITION SYSTEMS

In this section we briefly review a sample of the iris recognition literature with respect to the three basic modules. We pay particular attention at this point to iris location and preprocessing, feature extraction and signature encoding, and signature matching. Image acquisition is an interesting and important issue, but we do not address that issue here.

Perhaps the best known and most thoroughly tested algorithm is that of Daugman, see [1-3]. The Daugman algorithm first locates the pupillary and limbic boundaries of the iris using an integrodifferential operator that finds the circles in the image where the intensity is changing most rapidly with respect to changes in the radius. Once located, the iris image is converted to a Cartesian form by projecting it to onto a dimensionless pseudo-polar coordinate system. The iris features are encoded and a signature is created using a 2-D complex-valued Gabor filter, where the real and imaginary parts of each outcome are assigned a value of 0 or 1 according to whether they are negative or positive, i.e. only the quadrant of the phase is encoded. Finally, two images are said to be independent if their fractional Hamming distance (Hd) is above a certain threshold, about .33. Otherwise they are a match. Here, Hd equals number of mismatching bits divided by number of compared bits. The Daugman algorithm has been essentially error-free when applied to a very large database [3].

In [5], Tisse, et al., present a modification of Daugman's algorithm, with two major differences. The two innovations are in the iris location and feature extraction stages. The use of dimensionless polar coordinates and Hamming distance remain the same. To locate the iris, the Tisse algorithm applies a gradient decomposed Hough Transform to find the approximate center of the pupil, and then applies the integrodifferential operator, as in Daugman's algorithm, to find the precise locations of the iris boundaries. This combined approach has the advantage of avoiding errors due to specular reflection in the images. In the feature extraction and encoding step, the Hilbert Transform is used to create an *analytic image*, whose output is then encoded as an emergent frequency vector and an instantaneous phase. This approach has an advantage of being computationally efficient. The Tisse algorithm has reportedly been successful when tested on a database of real iris images [5].

Another well-known and thoroughly tested algorithm is due to Wildes [6]. The Wildes algorithm locates the iris boundaries by creating a binary edge map using gradient-based edge detection, and then finds the centers and radii of these circles via a Hough Transform. The upper and lower eyelids are located similarly using parabolic arcs. Rather than map every iris image to a common system of polar coordinates, the Wildes algorithm compares two images by geometrically warping one image, via shifting and rotation, until it is a best fit with the other image, in the sense of minimizing mean square distance. A Laplacian pyramid is constructed at four different resolution levels to encode the image data. Matching is achieved via an application of normalized correlation and Fisher's linear discriminant.

Boles and Boashash [7] have given an algorithm that locates the pupil center using an edge detection method, records grey level values on virtual concentric circles, and then constructs the zero-crossing representation on these virtual circles based on a one-dimensional *dyadic* wavelet transform. Corresponding virtual circles in different images are determined by rescaling the images to have a common iris diameter. The authors create two dissimilarity functions for the purposes of matching, one using every point of the representation and the other using only the zero crossing points. The algorithm has been tested successfully on a small database of iris images, with and without noise [7].

Several interesting ideas are presented by Lim, et al., in [8]. Following a standard iris localization and conversion to polar coordinates relative to the center of the pupil, the authors propose alternative approaches to both feature extraction and matching. For feature extraction they compare the use of the Gabor Transform and the Haar Wavelet Transform, and their results indicate to them that the Haar Transform is somewhat better. Using the Haar transform the iris patterns can be stored using only 87 bits, which compares well to the 2,048 required by Daugman's algorithm, for example. The matching process uses an LVQ competitive learning neural network, which is optimized by a careful selection of initial weight vectors. Also, a new multidimensional algorithm for *winner* selection is proposed. Experimental results are given in [8] based on a database of images of irises from 200 people.

An algorithm developed by Noh [9], et al., performs a comparison of different feature extraction techniques including Gabor wavelets, Haar wavelets, DAUB4 wavelets, Independent Component Analysis (ICA), and Mulitiresolution ICA (M-ICA). ICA is an unsupervised learning algorithm using high-order statistics, and M-ICA is a new method of feature extraction, introduced by these authors. The Fisher Discrimination Ratio is used as a comparison tool. Similar to the results mentioned by Lim, et. al, [9], the Haar wavelets had the best performance in their tests, followed closely by 2-D Gabor filters. The new M-ICA method performed well and further study is warranted.

Thoughtful and detailed discussions of iris recognition can be found in [10, 11], where Tan and his colleagues from China suggest several innovations, and then provide a comparison of different methods and algorithms. The the iris is localized in several steps which first find a good approximation for the pupil center and radius, and then apply the Canny operator and the Hough transform to locate the iris boundaries more precisely. The iris image is converted to dimensionless polar coordinates, similarly to Daugman, and then is processed using a variant of the Gabor filter. The dimension of the signature is reduced via an application of the Fisher linear discrimant. The L_1 distance, L_2 distance (i.e. Euclidean distance), and cosine similarity measures are considered for matching. A careful statistical performance evaluation is provided for the authors' work, and for most of the well-known algorithms mentioned above.

Several interesting ideas can also be found in the work of Du, et al., see [12]. The preprocessing stage is standard. Edge detection is performed using the Canny method, and each iris image is then transformed to standardized polar coordinates relative to the center of the pupil. The feature extraction stage is quite different from those mentioned previously, and is simple to implement. The authors use a gray scale invariant called Local Texture Patterns (LTP) that

compares the intensity of a single pixel to the average intensity over a small surrounding rectangle. The LTP is averaged in a specific way to produce the elements of a rotation invariant vector. Thus the method performs a lossy projection from 2D to 1D. This vector is then normalized so that its elements sum to 1. The matching algorithm uses the "Du measure", which is the product of two measures, one based on the tangent of the angle between two vectors p and q, and the other based on the relative entropy of q with respect to p, otherwise known as the Kullback-Liebler distance. Another paper involving Du [13], in the context of hyperspectral imaging, provides evidence that the Du measure is more sensitive than either of the other two measures. This iris recognition algorithm is quite fast and appears to be most appropriate for producing a "watchlist" [12], rather than being used for identification of specific individuals.

3. EXTENDING THE DEPTH-OF-FIELD

A key problem with existing approaches to iris signature acquisition is the limited depth-of-field of traditional imaging systems. In order to achieve reasonable lighting levels and exposure times, the optical system must have a high numerical aperture and a corresponding low F-number. Unfortunately, a high numerical aperture results in a corresponding small depth-of-field. Commercial iris recognition implementations typically require the user to move his or her head back and forth with respect to the camera until the focus quality is good enough to provide a sufficiently high contrast iris signature. Some implementations rely on audio cues and others rely on visual cues to let the user know when the iris is at an appropriate distance from the camera. The process can be time consuming and is an obstacle to acceptance of the process in daily use.

3.1 Computational imaging systems

A major component of our work has been to address the interaction between the image gathering method and the iris recognition algorithm. Prior work in iris recognition, as described in Section 2, has been predicated on the assumption of traditional image gathering techniques whose aim is to produce sharply focused and visually pleasing images. Our goal is to modify the image acquisition to maximize the information which is directly relevant to the recognition task.

To accomplish this goal, we have been investigating the use of specially designed optical aspheres for extending the depth-of-field of iris recognition imaging systems [14, 15]. Dowski and Cathey [16] have shown in 1995 that a particular phase encoding aspheric element (mask) has a remarkable ability to produce focus-invariant imagery. The mask is placed near the aperture stop of the image acquisition system and produces a blurred image, but the nature of the blur remains largely invariant over a wide range of defocus values (see Figure 2). We refer to such a system as a *computational imaging system*, since the imaging process includes a post detection processing stage. The authors of the current paper have recently been working on numerical optimization schemes to arrive at new mask surfaces that provide improved performance [14, 15, 17, 18, 21-25].

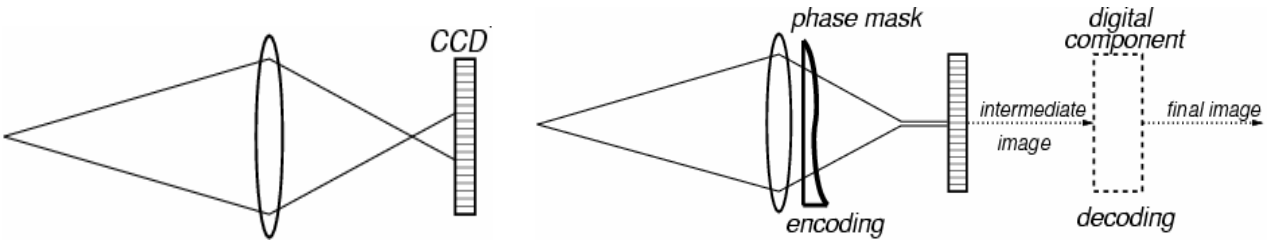

Figure 2: Graphical representation of (left) a standard imaging system , and (right) cubic phase modified imaging system.

The amount of phase deviation produced by an aspheric phase mask determines the amount of focus invariance. The phase profile of a general cubic phase encoding element [16] has its surface profile specified by

$$P(x, y) = \exp(i\alpha[x^3 + y^3]) \quad \text{for } |x| \le 1, |y| \le 1, \tag{1}$$

where we employ a dimensionless *x, y* coordinate system and the choice of α governs the overall phase thickness of the mask. Large values of α correspond to large phase deviations and yield high focus invariance at the expense of low modulation transfer function (MTF) values.

Representative images gathered with the standard imaging configuration are shown in Figure 3. Images gathered with the cubic are shown in Figure 4. The cubic aspheric phase mask available for all the experiments in this paper had a relatively small value of alpha of approximately 11 that is smaller than the recommended value of 20 or greater [17]. In practice, we find that operating with this small value still provides significant focus invariance while providing relatively high MTF values. Notice that the cubic images in Figure 4 display more iris texture for large values of defocus than do the defocused standard images. This is of particular importance for iris recognition purposes.

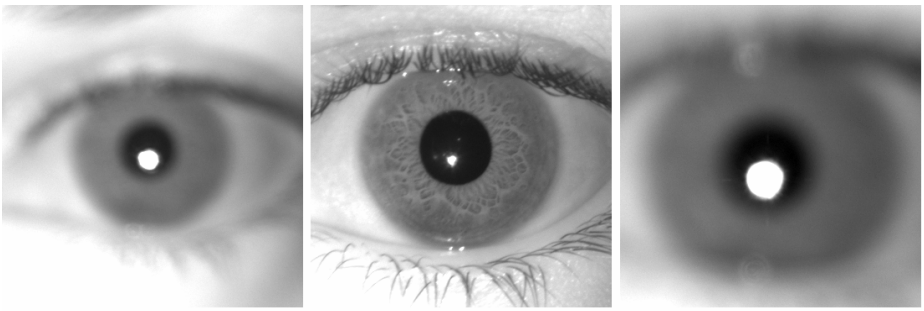

Figure 3: Laboratory gathered images using a standard imaging system at three focus positions: (a) -15 cm away from best focus, (b) best focus, and (c) +11 cm away from best focus. A negative number means that the iris is placed further from the camera compared to best focus. Note the light from the illumination reflected in the pupil.

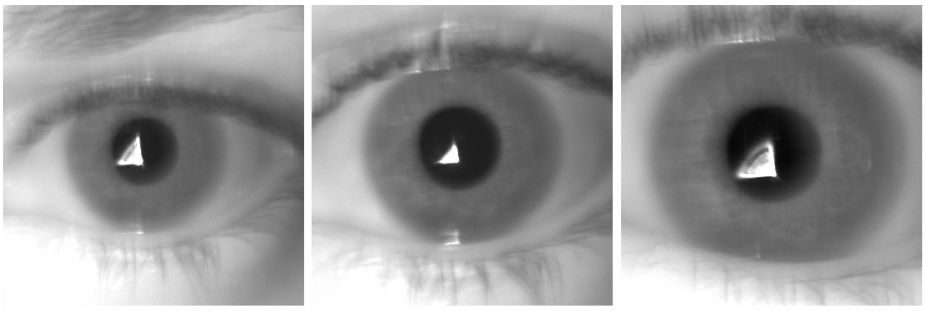

Figure 4: Laboratory gathered images using a cubic phase modified imaging system at three focus positions: (a) -15 cm away from best focus, (b) best focus, and (c) +11 cm away from best focus. A negative number means the iris is placed further from the camera compared to best focus. Note that the light from the illumination reflected in the pupil now exhibits the PSF form of the inserted phase mask.

The basic premise for both the laboratory and simulation experiments in this paper is to capture iris images both with a standard clear aperture imaging system and a computational imaging system, i.e. a system differing only by the insertion of aspheric phase element at the aperture stop of the image capture system. Clearly focused images captured without the phase mask are enrolled using the Daugman algorithm. Both standard and phase blurred images are captured over a large range of defocus and verified against the enrolled images. The goal is to determine whether computational imaging systems allow for successful recognition over a wider range of defocus.

3.2 Laboratory experimentation for extended volume acquisition

In this section, we provide a summary of our laboratory experimentation for determining whether computational imaging systems allow for successful iris recognition over a wider range of defocus. The full laboratory experiments are described in more detail elsewhere [14]. We have relied in part on a standard cubic phase mask, given by (1), for the image capture and in part on the Daugman algorithm for verification experiments. The best focused image in Figure 3 (center) was enrolled using the Daugman algorithm. The images were then verified against the enrolled best focused image. Figure 5(a) shows the recognition performance for the standard image gathering configuration. Daugman [2, 3]

recommends a Hamming distance threshold of approximately 0.33 for iris matches, where scores lower than 0.33 are considered as matches. The standard system performance is limited to approximately 10 to 15 cm of defocus range. Figure 5(b) shows that the iris matching scores of the cubic phase mask gathered imagery are at or below the threshold for more than 30 cm. Unfortunately, the iris scores are only slightly below the threshold.

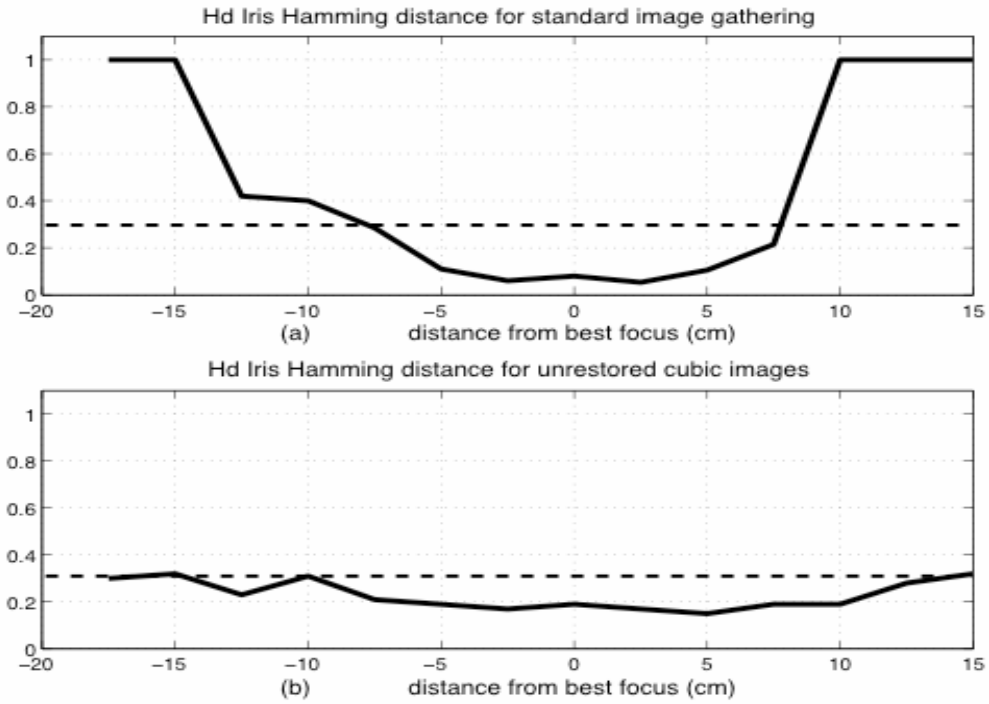

Figure 5: Iris recognition performance as a function of the physical distance from iris to camera for laboratory images captured, using (a) the standard imaging system and (b) a cubic phase encoded imaging system. The Hamming distance measures the difference between the iris template for an enrolled well-focused standard iris image and the candidate iris templates. Multiple candidate images of the same iris were captured at each camera position and the iris Hamming distances were averaged at each position. Values below the dashed line at 0.33 are considered matches. Due to a limitation in the algorithm implementation, mismatches having a score of Hd > 0.42 were thresholded to 1. No digital restoration was applied to the cubic system images.

The Daugman algorithm was originally designed for optimal performance assuming well-focused imagery. While the iris recognition results using phase mask blurred imagery provide extended depth-of-field, the overall quality of the matches as compared with well-focused imagery were poorer as evidenced by higher Hamming distance values. Digital image restoration can be applied to the blurred imagery to more closely approximate a well-focused image. We chose in these laboratory experiments to use a simple direct Wiener restoration approach, based upon the signal to noise ratio (SNR), to investigate the effect of image restoration on the performance of the algorithm. The Wiener restoration filter is described in the frequency domain as

$$W(u,v) = \frac{H^*(u,v)}{\left|H(u,v)\right|^2 + \left(\mathrm{SNR}\right)^{-2} \hat{\Phi}_N(u,v)/\hat{\Phi}_L(u,v)}, \tag{2}$$

where $H(u,v)$ is the imaging system transfer function including the effects of the imaging optics as well as the detector, $\hat{\Phi}_L(u,v)$ is the expected object power spectrum normalized to unit energy, $\hat{\Phi}_N(u,v)$ is the unit normalized electronic detection noise power spectrum, and SNR is the estimated root mean squared signal-to-noise ratio. In Section 3.3 we consider iterative methods for the restoration, and note the gain in Hamming distance performance at the expense of slightly more numerical computations.

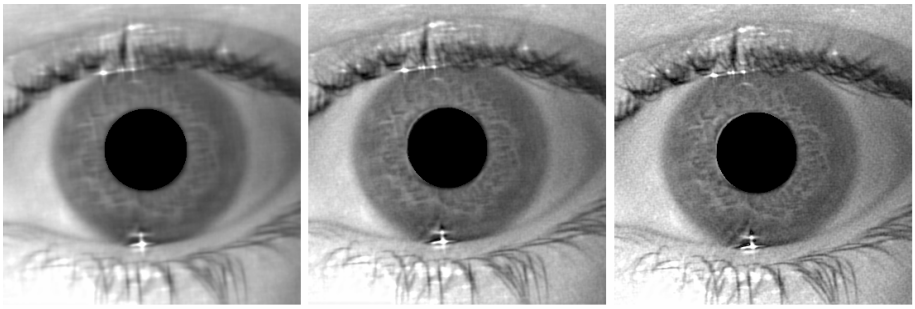

Figure 6: Restored images using Wiener filters under the assumption of different SNR (a) 50, (b) 200 and (c) 500. The pupil was artificially forced to zero after restoration to overcome difficulties in the iris boundary localization step in the iris segmentation stage.

The Wiener restoration approach produces more visually pleasing images as indicated in Figure 6. The restored image with the greatest amount of fine feature detail corresponds to the image Wiener filtered using an SNR assumption of 200. The restored image corresponding to SNR=50 is noticeably blurrier and less detailed or visually pleasing. The recognition results using restored imagery are shown in Figure 7. All three of the restoration filters produce improved iris scores compared with non-restored imagery, but the images corresponding to SNR=50 were slightly better than the sharper images produced using SNR=200 and SNR=500. These results corroborate Daugman's assertions [3] that only lower and middle frequencies contribute significantly to the iris code, and this directly verifies our simulation results.

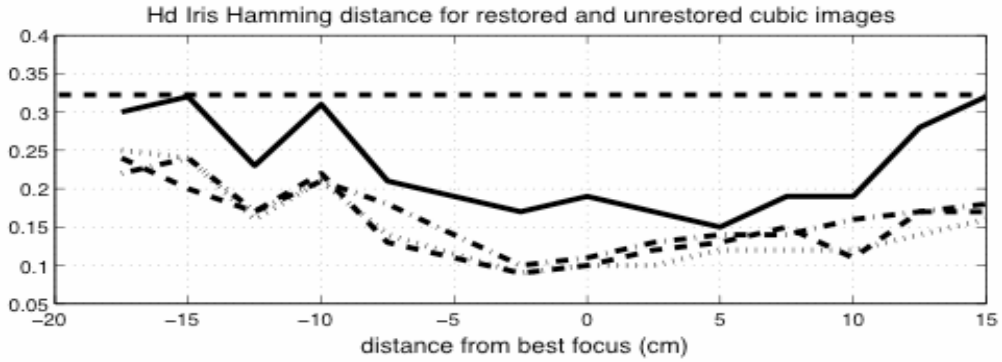

Figure 7: Iris recognition performance as a function of the physical distance from iris to camera for unrestored and restored cubic phase images. The Hamming distance measures the difference between the iris template for an enrolled well-focused standard iris image and the candidate iris templates. Legend: solid line is unrestored, dashed line is SNR=50, dotted line is SNR=200 and dashdot line is SNR=500.

This experimental laboratory work demonstrates that computational imaging can improve the performance of iris recognition over a large range of focus. Further performance benefits require a more general design procedure that considers other choices of the asphere phase mask in relation to the iris recognition algorithm being used.

3.3 Numerical simulation based experimentation for extended volume acquisition

In this section we report on our experimentation using numerically simulated blurred imagery for a standard imaging system as well as a computational imaging system, consistent with those used in laboratory experimentation for iris recognition. Our goal is three-fold: 1) to facilitate experimentation with much larger image datasets and in a shorter amount of time than can be possible in a laboratory setup, 2) to experiment with more effective restoration methods such as conjugate gradients least squares iteration, and 3) to support future experimentation with better optimized phase masks than just the cubic (see Section 4).

A dataset of 10 iris images was selected from a large dataset, obtained from Iridian Technologies, Inc., to represent a variety of practical situations such as amount of visible iris as well as placement and size of the specular blur. Each of the 10 selected iris images was registered so that the center of the pupil was located at the center of the image. This was important in order to more accurately simulate magnification and demagnification of the image due to varying distance from the plane of focus (see images in Figure 3). In other words, the object in an image is enlarged and reduced to simulate placement of the subject in a range between -20 and 20 centimeters from best focus, providing a total range of about 15 inches around a focal plane about 20 inches from the camera.

Direct linear methods such as the Wiener filter, and various related filtering approaches, can sometimes be effective for restoration of the intermediate iris image blurred by phase encoding, as illustrated in Section 3.1. However, exploring tradeoff space between blur and noise and the use of effective regularization involving the SNR is often difficult. Iterative methods allow for a more systematic process, with adaptive computation and expanded regularization options such as truncated iterations. For these and other reasons iterative techniques are now often the method of choice for image restoration computations. Our purpose here is to investigate the use of iterative methods for removing the cubic phase blur produced by (1). The method we consider is the conjugate gradient method for least squares (CGLS). This scheme is used extensively for solving large linear systems of equations, and has a nice property that we exploit in our problems; early termination of the iterations produces a regularized solution. (See [20] for details from an initial study on the use of CGLS for this application.)

The experimentation setup is as follows. The desired range of -20 to 20 centimeters from best focus is discretized in steps of 2.5cm, i.e. distances of d = -20, -17.5, -15,…, 0,…, 17.5, 20. For each value of d , the PSF is computed as,

$$h_{d,\alpha} = \left| F^{-1}\left\{ A \exp\left(i\pi (2w_d (x^2 + y^2) + \alpha (x^3 + y^3) \right) \right\} \right|$$

where the number of waves of defocus w_d is calculated based on the distance value d as well as on imaging system parameters such as wavelength of incident light, focal length, and the system's pupil diameter. The parameter α was set to 11 in order to simulate the phase mask used in our laboratory experimentation. The PSF is then used to blur a properly magnified image f using two-dimensional convolution,

$$g_d = h_{d,\alpha} \otimes f + \eta$$

where η is zero-mean white Gaussian additive noise. The resulting blurred image g_d is then restored using a conjugate gradient least squares iteration algorithm (CGLS) for up to thirty iterations. At each i-th iteration of CGLS the two-norm of the relative error as well as the Hamming distance between the computed solution f_i and the true image f are computed. This procedure is repeated for each of the 10 registered iris images and for three independent realizations of 2% (SNR=50) and 3% (SNR=33) noise. The Hamming distance values for all 10 iris images at each distance d are then averaged for each 2% and 3% noise. The results are shown in Figure 8.

Here, Figure 8 (top) shows the iris recognition performance for the standard gathering imaging system (α =0). Notice that the range of acceptability is only approximately 3cm larger in each direction than that obtained in the laboratory experimentation. A real system, like the one used in the laboratory tests reported in Section 3.1, introduces aberrations and other types of noise. For example, the actual lens system introduces spherical and other aberrations, which we know increases the Hamming distance [25, 26]. Figure 8 (bottom) shows the iris recognition performance for the cubic based computational imaging system for no restoration (solid line) and for CGLS restorations (average of the best Hamming distance value) for 2% and 3% noise. The better performance of CGLS with respect to the Wiener restorations in the previous section is expected since an optimal Hamming distance value can be found at each run of CGLS. This is in contrast to the "one-time shot" application of the Wiener filter.

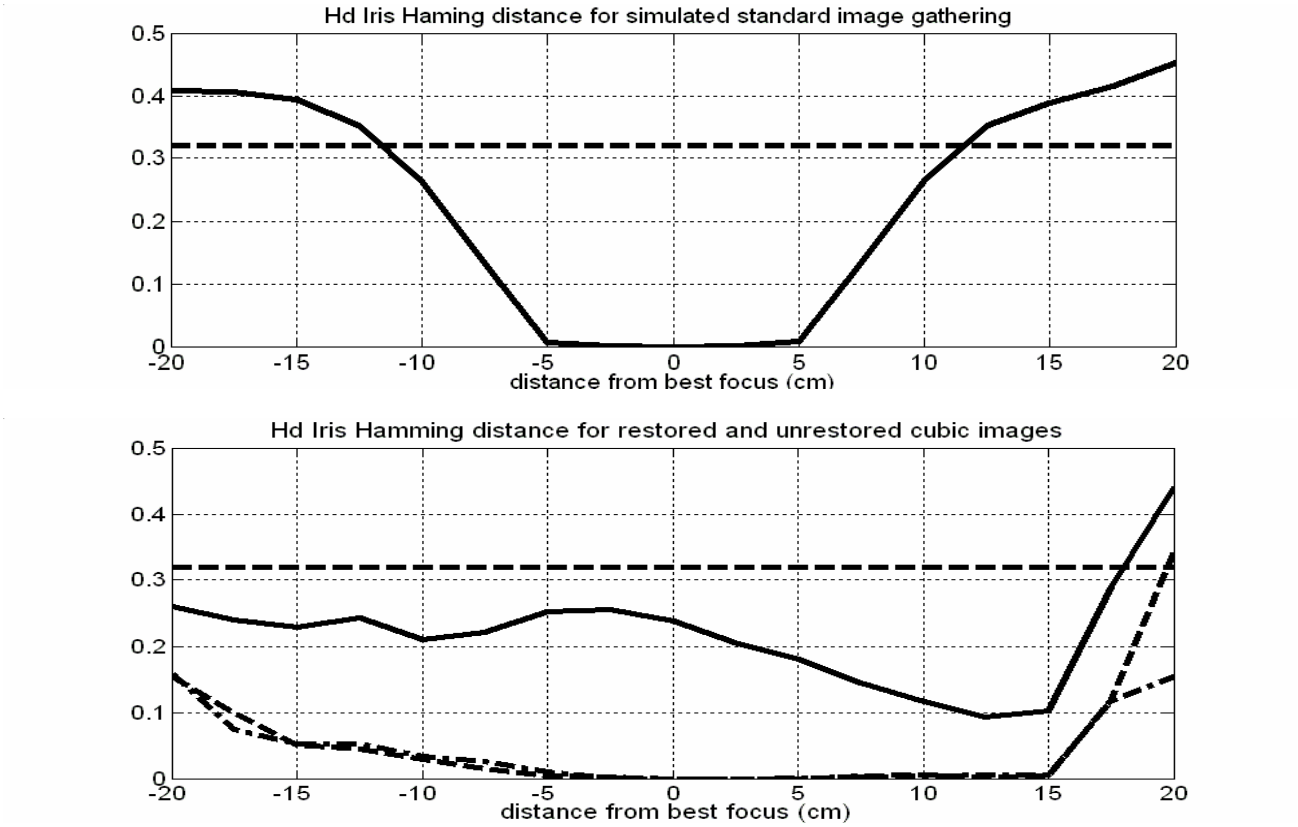

Figure 8: Iris recognition performance as a function of the physical distance from iris to camera, using (top) the standard imaging system and (bottom) a cubic phase encoded imaging system (Legend: solid line is for unrestored images with SNR=50, dashed line is for restored images with SNR=50, dashdot line is for restored images with SNR=33).

The Hamming distance value between two measures used in this paper corresponds to the number of mismatching bits Hd_raw divided by number of compared bits Hd_mod [26]. Hd_mod "normalizes" Hd_raw to a standard number of compared bits by increasing the Hamming distance when the number of compared bits is low and vice versa (similar to a z-score normalization). It is the Hd_mod that is used to determine match vs. mismatch in the tests to follow (specifically, Hd_mod < 0.33 means a match). We use Hd for Hd_mod for Figures 8 and 9.

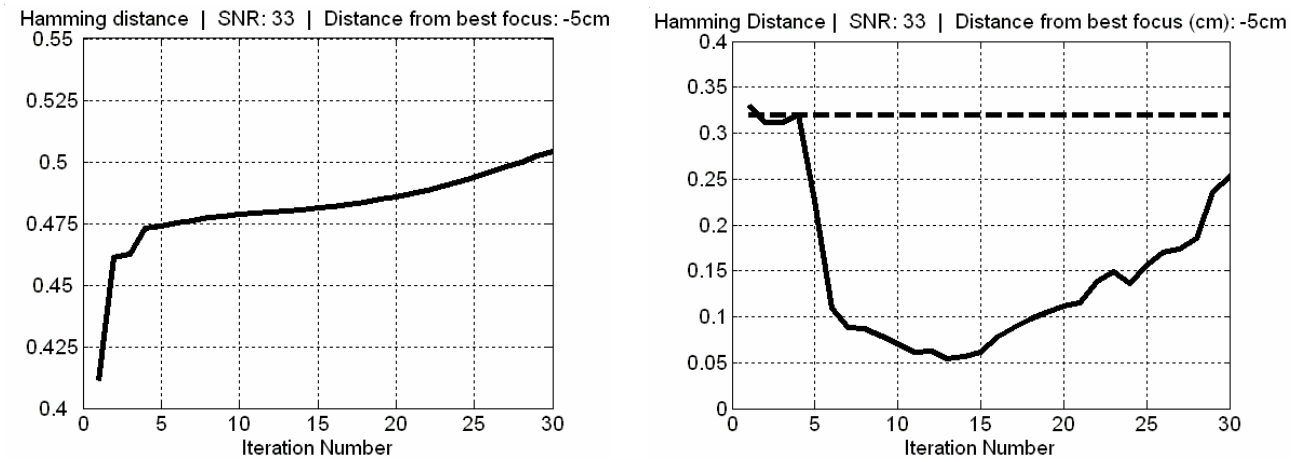

Figure 9: CGLS restoration performance in terms of (left) two-norm of the relative error, and (right) Hamming distance Hd.

The performance of CGLS, at each iteration, with respect to the two-norm of the relative error and the Hamming distance, is illustrated in Figure 9. Notice that the Hamming distance is improved from iterations 4 – 13, and remains acceptable through iteration 30, even though the relative error of the restored image increases slightly.

4. DESIGNING NEW COMPUTATIONAL IMAGING SYSTEMS

A critical requirement of a robust iris recognition system is a reliably high quality of the iris images it must routinely acquire both at the enrollment and authentication stages. To achieve this, the imaging system must possess a reasonably high depth-of-field and insensitivity to aberrations while allowing sufficient light throughput to record images accurately. Stopping down the aperture is not a viable option. While increasing the depth-of-field and reducing aberration, it reduces both the light flux and the native resolution of the images.

In recent years, some of the authors of this paper have applied information theoretic optimization approaches to improving the depth-of-field of a camera [14, 15, 17, 18, 21-25]. Called Wavefront Coding [16], the original idea sought via a simple modification of the pupil phase to decrease the sensitivity of the MTF of the optical system to misfocus errors. Although the images produced in this way have a lower quality than without any pupil-phase modifications, the depth insensitivity of the images permits them to be deconvolved in a space-invariant fashion and thus improve the overall resolution of the images without compromising the achieved depth insensitivity. One more general approach, called pupil-phase engineering (PPE), is a nonlinear optimization approach that seeks to determine the best pupil phase distribution that achieves a balance among various competing requirements of high SNR, sought depth-of-field, restorability, etc.

We may parameterize the pupil phase in a number of ways. The simplest, and perhaps least biased, phase profile $\psi(x, y)$ is symmetric under the interchange of x and y and is odd under inversion in the (x, y) plane, its oddness leading to a PSF whose Taylor expansion in the misfocus parameter has only even-power terms. Ignoring the linear terms, we take the phase to have the following form:

$$\Psi(x, y) = a(x^3 + y^3) + b(x^2 y + x y^2) + c(x^5 + y^5) + d(x^4 y + x y^4) + e(x^3 y^2 + x^2 y^3) + \ldots$$

This polynomial expansion for the phase is truncated at a finite number of terms and the values of the coefficients of the retained terms are optimized by means of one of a number of possible depth-extension/image restorability criteria. We have employed three different criteria in our past work: Insensitivity of Strehl ratio (on-axis PSF) to defocus [21, 22], Fisher-information-based insensitivity of the full PSF over the desired defocus range [23, 24], and a certain minimax optimization formulation [25] of the restorability of the phase-encoded image as measured by the integral of the MTF over allowed spatial frequencies. Technical details of these approaches are presented in [21-25]. Note that the PPE approaches to extend the depth-of-focus also automatically achieve improved performance against any geometrical (Seidel) aberrations, except possibly coma, of the optical imaging system, making it possible to relax the relative desirability of on-axis versus off-axis imaging of the iris. In other words, there is not just increased focal depth but an increased focal volume that results from these approaches. A quantitative estimation of the amount of focal-volume increase is postponed to future work. (See also [15].)

5. DISCUSSION

We have surveyed various biometric iris recognition systems and have described some new computational imaging approaches to iris recognition using phase encoding. These new approaches can greatly increase the depth-of-field over that possible with traditional optics, while keeping sufficient recognition accuracy. The combination of optics, detectors, and image processing all contribute to the iris recognition accuracy and efficiency. Various optimization methods for designing the optics and the image processing algorithms have been put forth, and we have provided laboratory and simulation results from applying these systems while restoring the intermediate phase encoded images, using direct Wiener filter and iterative conjugate gradient methods. One can infer that phase encoding provides:

- extended imaging volume (user cooperation becomes less necessary)
- robustness and reliability
- lower cost compared to other solutions (pan camera and auto-focus), and that

- electronic processing required by encoding and decoding the phase imposes small overhead compared to iris segmentation, iris code generation and iris score assessment.

New methods for post-processing the intermediate phase encoded image have been developed by the authors. In this work we have seen *excellent* iris score results by using restoration strategies that only enhance the lower frequencies. In particular, recent results with adjusting the bandwidth of the expected object spectrum in a Wiener filter as well as results with only a few conjugate gradient iterations are quite effective. In both cases, a key point is that the best restorations for iris do not generally agree with human subjective evaluations that place a premium on crispness and a visually appealing image. More details of these results are reported elsewhere, including [14, 24].

Current work underway includes comparison of specific iris recognition algorithms in the context of computational imaging systems, including algorithms by Daugman [1-3], by Tisse, et al., [5], and by Du, et al., [12]. These comparisons are in combination with phase encoding for extended imaging volume and for removing certain imaging system aberrations such as spherical aberration.

ACKNOWLEDGMENTS

This work was accomplished with the support of the Army Research Office under DOD Grant # DAAD19-00-1-0540. Iridian Technologies, Inc. provided us with executable software for an implementation of the Daugman iris recognition algorithm under a Cooperative Research and Development Agreement (CRADA) with Wake Forest University. We would also like to thank Ulf Cahn von Seelen and James Cambier of Iridian Technologies, Inc. as well as John Daugman of Cambridge University for many helpful discussions concerning the iris recognition algorithm.

REFERENCES

1. J. G. Daugman, “High confidence visual recognition of person by a test of statistical independence,” *IEEE Trans. PAMI* **15**, 1148-1161 (1993).

2. J. G. Daugman, "The importance of being random: statistical principles of iris recognition," *Patern. Recognition* **36**, 279-291 (2003).

3. J. G. Daugman, “How iris recognition works,” *IEEE Trans. Circuits and Syst. for Video Tech*. **14**(1), 21-30 (2004).

4. E. Wolf, *Anatomy of the Eye and Orbit*, 7th Edition, H. K. Lewis & Co. LTD, 1976.

5. C. Tisse, L. Martin , L. Torres, and M. Robert, “Iris recognition system for person identification,” *PRIS 2002* : 186-199 (2002).

6. R. P. Wildes, “Automated iris recognition: An emerging biometric technology,” *Proceedings of the IEEE* **85** 1348-1363 (1997).

7. W. Boles, and B. Boashash, “A human identification technique using images of the iris and wavelet transform,” *IEEE Trans. Signal Proc*. **4**:1185-1188, (1998).

8. S. Lim, K. Lee, O. Byeon, and T. Kim, “Efficient iris recognition through improvement of feature vector and classifier,” *ETRI J*. **23**(2):61-70, (2001).

9. S-I. Noh, K. Pae, C. Lee, and J. Kim, “Multiresolution independent component analysis for iris identification,” *Proc. International Conf. on Circuits/Systems Computers and Communications*, Phuket, Thailand, (2002).

10. Y. Zhu, T. Tan, and Y. Wang, "Biometric personal identification based on iris pattern,” *ICPR2000: the 15th International Conference on Pattern Recognition*, Barcelona, Spain, 805-808, (2002).

11. L. Mai, T. Tan, Y. Wang, and D. Zhang, "Personel identification based on iris texture analysis," *IEEE Trans. on Pattern Analysis and Machine Intelligence* **25**(12):1519-1533, (2003).

12. Y. Du, R. Ives, C-I. Chang, D. Etter, and T. Welch, "Information divergence-based iris pattern recognition for automatic human identification," (to be published) *Proc. SPIE* **5404**, 2004.

13. Y. Du, R. Ives, C-I. Chang, H. Ren, F. D'Amico, and J. Jensen, "A new hyperspectral discrimination measure for spectral similarity," *Optical Engineering* **43**(8), (2004).

14. J. van der Gracht, V. P. Pauca, H. Setty, E. R. Dowski, R. J. Plemmons, T. C. Torgersen, and S. Prasad, "Iris recognition with enhanced depth-of-field image acquisition," (to be published) *Proc. SPIE* **5358**, 2004.

15. R. Narayanswamy, G. E. Johnson, Paulo E. X. Silveira, and H. B. Wach, "Extending the Imaging Volume for Biometric Iris Recognition," (to be published) *Applied Optics*, Feb. 2005.

16. E. Dowski, and W. Cathey, "Extended depth of field through wavefront coding," *Appl. Opt.* **34**:1859-1866, (1995).

17. W. Cathey, and E. Dowski, "A new paradigm for imaging systems," *Applied Optics,* **41**, 6080, (2002).

18. E. Dowski, and K. Kubala, "Modeling of wavefront coded imaging systems," *Proc. SPIE* **4736**, 116-126, (2003).

19. J. van der Gracht, E. Dowski, M. Taylor, and D. Deaver, "Broadband behavior of an optical-digital focus-invariant system," *Opt. Lett*. **21**, 919-921 (1996).

20. J. van der Gracht, J.G. Nagy, V.P. Pauca, and R.J. Plemmons, "Iterative restoration of wavefront coded imagery for focus invariance," *OSA Trends in Optics and Photonics (TOPS), Integrated Computational Imaging Systems, OSA Technical Digest*, 2-4 (2001).

21. S. Prasad, T.C. Torgersen, V. P. Pauca, R. J. Plemmons, and J. van der Gracht, "Engineering the pupil phase to improve image quality," *Proc. SPIE* **5108**, 1-12, (2003).

22. S. Prasad, T. Torgersen, V. P. Pauca, R. J. Plemmons, and J. van der Gracht, "Restoring Images with Space Variant Blur via Pupil Phase Engineering," *Optics in Info. Systems, Special Issue on Comp. Imaging* **4**(2), 4-5, (2003).

23. P. Pauca, S. Prasad, R. J. Plemmons, T. C. Torgersen, and J. van der Gracht, "Integrated Optical-digital approaches for enhancing image restoration and focus invariance," *Proc. SPIE* **5205**, 348-357, (2003).

24. S. Prasad, T. C. Torgersen, V. P. Pauca, R. J. Plemmons, and J. van der Gracht, "High-Resoultion Imaging Using Integrated Optical Systems," (to be published) *International J. of Imaging Systems and Technology*, Aug. 2004.

25. S. Prasad, V. P. Pauca, R. J. Plemmons, T. C. Torgersen, and J. van der Gracht, "Pupil-phase optimization for extended-focus, aberration-corrected imaging systems," (to be published in this volume) *Proc. SPIE* **5559**, 2004.

26. Ulf Cahn von Seelen, "Personal correspondence", Iridian Technologies, Inc., May 2004.